

AD-A226 581

DTIC FILE COPY

2

OFFICE OF NAVAL RESEARCH

CONTRACT NO. N00014-86-K-0545

TECHNICAL REPORT NO. 12

SEP 17 1990  
S  
D  
E

FTIR STUDIES OF H<sub>2</sub>O AND D<sub>2</sub>O DECOMPOSITION ON POROUS SILICON SURFACES

P.Gupta, A.C. Dillon, A.S. Bracker and S.M. George

Submitted to  
Surface Science

Reproduction in whole or in part is permitted for any purpose of the United States Government.

This document has been approved for public release and sale, its distribution is unlimited

## REPORT DOCUMENTATION PAGE

1a. REPORT SECURITY CLASSIFICATION Unclassified		1b. RESTRICTIVE MARKINGS	
2a. SECURITY CLASSIFICATION AUTHORITY		3. DISTRIBUTION/AVAILABILITY OF REPORT Approved for public release: Distribution unlimited	
2b. DECLASSIFICATION/DOWNGRADING SCHEDULE		4. PERFORMING ORGANIZATION REPORT NUMBER(S) Technical Report No. 12	
5. MONITORING ORGANIZATION REPORT NUMBER(S) 12		6a. NAME OF PERFORMING ORGANIZATION Department of Chemistry Stanford University	
6b. OFFICE SYMBOL (if applicable)		7a. NAME OF MONITORING ORGANIZATION Office of Sponsored Projects Stanford University	
6c. ADDRESS (City, State, and ZIP Code) Stanford, California 94305-5080		7b. ADDRESS (City, State, and ZIP Code) Stanford, California 94305	
8a. NAME OF FUNDING/SPONSORING ORGANIZATION Office of Naval Research		8b. OFFICE SYMBOL (if applicable)	
9. PROCUREMENT INSTRUMENT IDENTIFICATION NUMBER N00014-86-K-0545		8c. ADDRESS (City, State, and ZIP Code) Chemistry Division 800 N. Quincy Street Arlington, VA 22217-5000	
10. SOURCE OF FUNDING NUMBERS		11. TITLE (Include Security Classification) FTIR Studies of H <sub>2</sub> O and D <sub>2</sub> O Decomposition on Porous Silicon Surfaces	
PROGRAM ELEMENT NO.	PROJECT NO.	TASK NO.	WORK UNIT ACCESSION NO.
12. PERSONAL AUTHOR(S) P. Gupta, A.C. Dillon, A.S. Bracker and S.M. George		13a. TYPE OF REPORT Interim/Technical	
13b. TIME COVERED FROM _____ TO _____		14. DATE OF REPORT (Year, Month, Day) 90/31/07	
15. PAGE COUNT		16. SUPPLEMENTARY NOTATION	
17. COSATI CODES		18. SUBJECT TERMS (Continue on reverse if necessary and identify by block number)	
FIELD	GROUP	SUB-GROUP	
19. ABSTRACT (Continue on reverse if necessary and identify by block number) The decomposition of H <sub>2</sub> O and D <sub>2</sub> O on silicon surfaces was studied using transmission Fourier-Transform Infrared (FTIR) spectroscopy. These FTIR studies were performed in-situ in an ultra-high vacuum chamber using high surface area porous silicon samples. The FTIR spectra revealed that H <sub>2</sub> O (D <sub>2</sub> O) initially dissociates upon adsorption at 300 K to form SiH (SiD) and SiOH (SiOD) surface species, i.e. H <sub>2</sub> O → SiH + SiOH. The decomposition of these surface species was then monitored using the Si-H (Si-D) stretch at 2100 cm <sup>-1</sup> (1518 cm <sup>-1</sup> ), SiO-H (SiO-D) stretch at 3680 cm <sup>-1</sup> (2713 cm <sup>-1</sup> ) and the Si-O-Si stretch at 900 - 1100 cm <sup>-1</sup> . As the silicon surface was annealed to 650 K, the FTIR spectra revealed that the SiOH surface species progressively decomposed to Si-O-Si species and additional SiH species, i.e. SiOH → SiH + SiOSi. Above 650 K, the SiH surface species decreased concurrently with the desorption of H <sub>2</sub> from the porous silicon surface. New blue-shifted infrared features in the Si-H stretching region were observed at 2119 cm <sup>-1</sup> , 2176 cm <sup>-1</sup> and 2268 cm <sup>-1</sup> after annealing above 600 K. Additional infrared studies of partially hydrogen-covered porous silicon surfaces CHEMICAL REACTIONS, JS) CONTINUED ON REVERS SIDE...			
20. DISTRIBUTION/AVAILABILITY OF ABSTRACT <input checked="" type="checkbox"/> UNCLASSIFIED/UNLIMITED <input type="checkbox"/> SAME AS RPT. <input type="checkbox"/> DTIC USERS		21. ABSTRACT SECURITY CLASSIFICATION Unclassified	
22a. NAME OF RESPONSIBLE INDIVIDUAL Dr. David L. Nelson / Dr. Mark Ross		22b. TELEPHONE (Include Area Code) (202) 696-4410	
		22c. OFFICE SYMBOL	



**FTIR Studies of H<sub>2</sub>O and D<sub>2</sub>O Decomposition on Porous Silicon Surfaces**

**P. Gupta, A.C. Dillon, A.S. Bracker and S.M. George**  
Department of Chemistry,  
Stanford University,  
Stanford, California 94305

**Abstract**

The decomposition of H<sub>2</sub>O and D<sub>2</sub>O on silicon surfaces was studied using transmission Fourier-Transform Infrared (FTIR) spectroscopy. These FTIR studies were performed *in-situ* in an ultra-high vacuum chamber using high surface area porous silicon samples. The FTIR spectra revealed that H<sub>2</sub>O (D<sub>2</sub>O) initially dissociates upon adsorption at 300 K to form SiH (SiD) and SiOH (SiOD) surface species, i.e. H<sub>2</sub>O → SiH + SiOH. The decomposition of these surface species was then monitored using the Si-H (Si-D) stretch at 2100 cm<sup>-1</sup> (1518 cm<sup>-1</sup>), SiO-H (SiO-D) stretch at 3680 cm<sup>-1</sup> (2713 cm<sup>-1</sup>) and the Si-O-Si stretch at 900 - 1100 cm<sup>-1</sup>. As the silicon surface was annealed to 650 K, the FTIR spectra revealed that the SiOH surface species progressively decomposed to Si-O-Si species and additional SiH species, i.e. SiOH → SiH + SiOSi. Above 650 K, the SiH surface species decreased concurrently with the desorption of H<sub>2</sub> from the porous silicon surface. New blue-shifted infrared features in the Si-H stretching region were observed at 2119 cm<sup>-1</sup>, 2176 cm<sup>-1</sup> and 2268 cm<sup>-1</sup> after annealing above 600 K. Additional infrared studies of partially hydrogen-covered porous silicon surfaces exposed to O<sub>2</sub> suggested that these blue-shifted Si-H stretching vibrations were associated with silicon surface atoms backbonded to one, two or three oxygen atoms, respectively.

90 01 1 006

## I. Introduction

The decomposition of H<sub>2</sub>O on silicon is a prototypical silicon surface reaction. The details of H<sub>2</sub>O adsorption are important for an understanding of chemisorption on silicon surfaces. The mechanism of H<sub>2</sub>O decomposition may also affect the quality of insulating silicon oxide layers produced by wet oxidation during semiconductor device processing.

Previous work on H<sub>2</sub>O chemisorption on silicon surfaces has focused on whether the adsorption is dissociative or nondissociative. Previous ultraviolet photoemission spectroscopy (UPS) results suggested that the chemisorption of H<sub>2</sub>O occurred non-dissociatively on Si(111) 7x7 (1). These studies were in agreement with older high-resolution electron energy loss spectroscopy (HREELS) studies of H<sub>2</sub>O on Si(111) 7x7 (2,3).

In contrast, more recent HREELS studies have observed silicon-hydrogen and silicon-hydroxyl species after H<sub>2</sub>O adsorption on Si(111) 7x7 at room temperature (4,5). Recent UPS (6) experiments and ellipsometric (7) studies have suggested that water chemisorbs dissociatively on Si(111) 7x7 at room temperature. Additional HREELS and infrared results for water adsorption on Si(111) 2 X 1 (8,9) and Si(100) 2 X 1 (6,9-11) have also provided evidence for dissociative H<sub>2</sub>O chemisorption.

Fourier transform infrared (FTIR) spectroscopy is sensitive to surface molecular structure and can resolve closely-spaced vibrational features. Moreover, transmission FTIR studies can probe the infrared region below 1200 cm<sup>-1</sup> that is obscured in multiple total-internal-reflection infrared experiments because of silicon lattice absorption (11-13). Numerous low frequency vibrational modes in this infrared region yield valuable structural information.

Because of sensitivity requirements, transmission FTIR spectroscopic studies are limited to high surface area materials. Given typical infrared cross sections of  $\sigma = 1 \times 10^{-18} \text{ cm}^2$  (14), single crystal silicon samples with  $1 \times 10^{15} \text{ surface-atoms/cm}^2$  do not have a sufficient surface area for facile transmission infrared studies. However, porous silicon can be utilized to obtain high-surface

area, crystalline silicon samples.

Porous silicon was first obtained by Uhlir (15) and Turner (16) by anodizing single-crystal silicon in dilute hydrofluoric acid. Transmission electron microscopy (TEM) micrographs have shown that porous silicon made from p-doped silicon contains a network of nearly parallel pores (17). These pores are approximately 20- 100 Å in diameter with a center-to-center separation of approximately the same magnitude (17). Likewise, Brunauer-Emmett-Teller (BET) model methods have measured extremely high surface areas of approximately  $200 \text{ m}^2/\text{cm}^3$  for porous silicon (18).

Other material properties of porous silicon have recently been characterized extensively (19-22). Under ordinary preparation conditions, porous silicon retains the crystallinity of the original silicon wafer (23-25). The crystallinity of porous silicon allows epitaxial layers of silicon to be grown on porous silicon using molecular beam epitaxy (MBE) techniques (26).

Porous silicon also exhibits sharp and pronounced infrared absorption features that can be assigned unambiguously to silicon monohydride and dihydride surface species (27). The desorption kinetics of  $\text{H}_2$  from monohydride (SiH) and dihydride ( $\text{SiH}_2$ ) species on porous silicon have recently been measured (27). These  $\text{H}_2$  desorption kinetic studies were in excellent agreement with the desorption kinetics of  $\text{H}_2$  from Si(111) 7x7 single crystal surfaces (28, 29).

In this study, transmission FTIR techniques were used to investigate the species formed after exposing porous silicon surfaces to a saturation  $\text{H}_2\text{O}$  or  $\text{D}_2\text{O}$  exposure. The thermal stability of the surface reaction species was measured by monitoring the Si-H (Si-D) stretch at  $2100 \text{ cm}^{-1}$  ( $1518 \text{ cm}^{-1}$ ), SiO-H (SiO-D) stretch at  $3680 \text{ cm}^{-1}$  ( $2713 \text{ cm}^{-1}$ ) and the Si-O-Si stretch at  $900 - 1100 \text{ cm}^{-1}$  as a function of surface temperature. These FTIR studies established that  $\text{H}_2\text{O}$  adsorption on silicon surfaces at 300 K is dissociative. The SiOH surface reaction intermediate was observed to decompose to SiOSi and SiH surface species between 400 - 600 K. In addition, new blue-shifted infrared features in the Si-H stretching region were monitored after SiOH decomposition and assigned to SiH species backbonded to oxygen atoms.

## II. Experimental

### A. Preparation of Porous Silicon

The electrochemical techniques used to prepare porous silicon have been described previously (27). These studies employed single-crystal Si(100) wafers with a thickness of 400  $\mu\text{m}$ . These silicon samples were *p*-type boron-doped with a resistivity of  $\rho = 0.19 \Omega \text{ cm}$ . The electrolyte consisted of a 38% Hydrofluoric acid-ethanol mixture. The anodization reaction was performed for 15 s with a constant current of 200  $\text{mA}/\text{cm}^2$ . This current flux and time corresponded to a total charge of 1.12  $\text{C}/\text{cm}^2$ .

In agreement with previous studies (24,27), the porous silicon samples produced using the above conditions were bluish-grey in color. The thickness of the porous silicon layer was approximately 2  $\mu\text{m}$ . Given a surface area of 200  $\text{m}^2/\text{cm}^3$ , the 2  $\mu\text{m}$  thick porous silicon layer provided a surface area enhancement of 400.

### B. UHV Chamber for Transmission FTIR Studies

Prior to mounting the porous silicon sample in the UHV chamber, the sample was rinsed successively in ethanol, acetone, trichloroethylene and hydrofluoric acid. The hydrofluoric acid was used to remove any native oxide that may have formed on the porous silicon surfaces after anodization. The samples were then mounted at the bottom of a liquid-nitrogen-cooled cryostat on a differentially-pumped rotary feedthrough (30). The crystal mounting design and techniques for sample heating have been described previously (27).

The UHV chamber for *in-situ* transmission FTIR studies was similar to the UHV chamber employed earlier (27). The UHV chamber was pumped by a 190 l/sec Balzers turbomolecular pump that was backed by another 50 l/sec turbomolecular pump. This tandem turbomolecular pump enabled pressures of  $2.0 \times 10^{-8}$  Torr to be obtained within 2 hr. after breaking vacuum. An isolation valve between the sample introduction chamber and the rest of the chamber facilitated this rapid recovery time when changing samples.

A Nicolet 740 FTIR spectrometer and an MCT-B infrared detector were employed in these studies. The infrared beam passed through a pair of 0.5 inch thick CsI windows on the vacuum chamber. Lower infrared frequencies were transmitted and higher optical throughput was obtained with CsI windows compared with the earlier ZnSe windows (27). The O-ring seals on the CsI salt windows limited the typical operating pressures to  $1 \times 10^{-8}$  Torr.

### C. Adsorption and Thermal Annealing Experiments

The surface species produced during  $H_2O$  ( $D_2O$ ) adsorption were studied as a function of water exposure and silicon surface temperature. In these experiments, the silicon substrate was held at a constant temperature. FTIR spectra were recorded versus water exposure until a saturation coverage was obtained. Adsorption as a function of exposure time was measured at isothermal temperatures between 300 K-800 K. The FTIR spectra were monitored at the adsorption temperature for temperatures between 300 - 500 K. Because of increased infrared absorption by free carriers at higher temperatures (31-33), FTIR spectra were recorded at 500 K for the isothermal adsorption experiments at temperatures above 500 K.

For the thermal annealing studies, porous silicon samples at 300 K were exposed to  $H_2O$  ( $D_2O$ ) until a saturation coverage was obtained.  $H_2O$  ( $D_2O$ ) exposures at  $1 \times 10^{-5}$  Torr for 20 minutes were employed to achieve a saturation coverage. The silicon surface temperature was then increased to the annealing temperature using a heating rate of 7 K/sec. The sample was held at the annealing temperature for approximately 1 min. Subsequently, the sample was returned to the initial temperature of 300 K before recording the FTIR spectra. This experimental sequence was performed repeatedly for annealing temperatures up to 800 K.

A new porous silicon sample prepared under identical conditions was used for each set of annealing experiments. The total concentrations of monohydride and dihydride species present initially on the porous silicon surface were the same within  $\pm 5\%$  for each sample. To obtain a clean surface before a water exposure, the porous silicon sample was annealed in vacuum to remove the surface hydrogen. The procedure consisted of annealing the porous silicon at 640 K for

4 minutes, followed by annealing at 800 K for an additional 4 minutes. Previous hydrogen desorption studies have shown that this annealing procedure is sufficient to remove hydrogen from both surface monohydride and dihydride species (27).

### III. Results

The infrared spectra of porous silicon after saturation  $\text{H}_2\text{O}$  and  $\text{D}_2\text{O}$  exposures at 300K are shown in Figs. 1 and 2, respectively. After a  $\text{H}_2\text{O}$  saturation exposure, the infrared spectrum displayed in Fig. 1 exhibited pronounced absorption features at  $3680\text{ cm}^{-1}$ ,  $2090\text{ cm}^{-1}$ ,  $775\text{ cm}^{-1}$  and  $620\text{ cm}^{-1}$ . After a  $\text{D}_2\text{O}$  saturation exposure, Fig. 2 reveals that infrared absorption features were observed at  $2707\text{ cm}^{-1}$ ,  $1513\text{ cm}^{-1}$ ,  $835\text{ cm}^{-1}$  and  $620\text{ cm}^{-1}$ . In addition, absorptions were also observed at  $2090\text{ cm}^{-1}$  and  $620\text{ cm}^{-1}$  because of some hydrogen isotopic exchange of  $\text{D}_2\text{O}$ .

After a saturation water exposure, changes in the infrared absorption spectrum of porous silicon versus annealing temperature are shown in Figs. 3 and 4. Fig. 3a shows the decrease in the infrared absorption of the Si-O-H stretch at  $3680\text{ cm}^{-1}$  versus annealing from 300K to 640K after a saturation  $\text{H}_2\text{O}$  exposure at 300 K. Fig. 3b shows the concurrent increase in the absorption of the Si-H stretch at  $2100\text{ cm}^{-1}$  over the same temperature range.

Figure 4 shows the corresponding growth of the infrared absorption at approximately  $980\text{ cm}^{-1}$  assigned to the Si-O-Si asymmetric stretch (34-36). Figure 4 also displays the concurrent decrease of the infrared absorption at  $835\text{ cm}^{-1}$  identified with the Si-OD stretching vibration. Because of an Si-H bending absorption feature that overlaps the Si-OH stretching vibration at  $775\text{ cm}^{-1}$ , the spectra in Fig. 4 were obtained after a saturation exposure of  $\text{D}_2\text{O}$ .

The integrated infrared absorbances versus annealing temperature after saturation  $\text{H}_2\text{O}$  and  $\text{D}_2\text{O}$  exposures at 300 K are displayed in Fig. 5 and Fig. 6, respectively. An increase by a factor of approximately 2 in the integrated absorbance for the Si-H and Si-D stretching vibrations is observed as the temperature is increased from 300 - 650 K. At temperatures higher than 650 K, the integrated absorbance decreases for both Si-H and Si-D stretching vibrations. This decrease is

consistent with the desorption of  $H_2$  or  $D_2$  from the silicon surface (27-29).

Figures 5 and 6 also reveal that the SiO-H and SiO-D stretching vibrations corresponding to SiOH and SiOD surface species have been removed from the surface after annealing above 650 K. The decrease in the integrated absorbance of the SiO-H and SiO-D stretching vibrations is correlated with the increase in the integrated absorbance of the Si-H and Si-D stretching vibrations. An increase in the integrated absorbance of the Si-O-Si stretch at  $900\text{ cm}^{-1}$  -  $1100\text{ cm}^{-1}$  is also concurrent with the increase of the SiH surface species.

The integrated absorbances of the Si-H stretching vibration versus  $H_2O$  exposure at 300 K and 600 K are displayed in Fig. 7.  $H_2O$  dissociative chemisorption as measured by the SiH surface species is characterized by a rapid initial  $H_2O$  adsorption rate. This rapid adsorption rate is then followed by progressively decreasing adsorption rates that ultimately lead to a saturation coverage after large  $H_2O$  exposures. Figure 7 reveals that the saturation hydrogen coverage is very dependent on surface temperature. The saturation hydrogen coverage at 600 K was approximately twice the saturation hydrogen coverage obtained at 300 K.

Fig. 8 shows the growth of the silicon oxide coverage versus  $H_2O$  exposure at 600 K and 800 K. The silicon oxide coverage was obtained by integrating the Si-O-Si asymmetric stretch at  $900\text{ cm}^{-1}$  -  $1100\text{ cm}^{-1}$ . Fig. 8 reveals that saturation oxide coverage obtained at 800 K is approximately five times the saturation oxide coverage obtained at 600K.

As the porous silicon was annealed, new blue-shifted infrared features were observed in the Si-H stretching region. Fig. 9a is an infrared spectra of porous silicon in the Si-H stretching region after a saturation  $H_2O$  exposure at 300 K. The Si-H stretching vibration is observed at  $2087\text{ cm}^{-1}$ . Fig 9b shows the infrared spectra of the same porous silicon sample after annealing to 640 K. The Si-H vibrational stretch has shifted to  $2102\text{ cm}^{-1}$ . Additional blue-shifted absorption features are also observed at  $2119\text{ cm}^{-1}$ ,  $2176\text{ cm}^{-1}$  and  $2268\text{ cm}^{-1}$ .

Fig. 10 displays infrared spectra obtained after a partially hydrogen-covered porous silicon surface was exposed to  $1 \times 10^{-5}$  Torr of  $O_2$  for 7 min. at 600 K. The initial hydrogen coverage on the porous silicon was  $0.27\Theta_s$ , where  $\Theta_s$  is the saturation coverage of hydrogen on porous silicon.

The infrared spectra exhibited new blue-shifted absorption peaks in the Si-H stretching region at  $2176\text{ cm}^{-1}$  and  $2269\text{ cm}^{-1}$  as shown in Fig. 10a and in the Si-H bending region at  $777, 820\text{ cm}^{-1}$ ,  $857\text{ cm}^{-1}$  as displayed in Fig. 10b.

## IV. Discussion

### A. Infrared Spectrum after Water Exposure

Reflectance infrared studies of hydrogen on Si(100) have assigned infrared features between  $2100 - 2080\text{ cm}^{-1}$  to Si-H vibrational stretching modes (37,38). After anodization, porous silicon exhibits two absorption peaks between  $2087 - 2110\text{ cm}^{-1}$ . Thermal annealing studies (27) have assigned these two absorption features to silicon dihydride and silicon monohydride stretching vibrations. The presence of silicon dihydride species on the anodized porous silicon surface is also confirmed by the  $\text{SiH}_2$  scissor mode at  $910\text{ cm}^{-1}$  (27). As the dihydride is removed from the surface, the monohydride peak at  $2110\text{ cm}^{-1}$  shifts to  $2102\text{ cm}^{-1}$  (27).

Figure 1 does not show any infrared absorption from a possible  $\text{SiH}_2$  scissors mode at  $910\text{ cm}^{-1}$ . This absence suggests that the  $2090\text{ cm}^{-1}$  feature after a  $\text{H}_2\text{O}$  saturation exposure is produced by a silicon-monohydride species on the surface. The corresponding deformation mode of the SiH species is observed at  $625\text{ cm}^{-1}$  in agreement with previous infrared studies on porous silicon (27) and HREELS investigations on Si(100) 2 X 1 (39). The infrared feature at  $1513\text{ cm}^{-1}$  in Fig. 2 is assigned to a Si-D stretching vibration. The Si-D deformation mode would be at  $480\text{ cm}^{-1}$  which is below the low frequency cutoff of the MCT-B infrared detector.

HREELS studies of water adsorption on Si(111) 2 X 1 (40), Si(111) 7 X 7 (4, 5), Si(100) 2 X 1 (5) and multiple total-internal-reflectance infrared studies of  $\text{H}_2\text{O}$  on Si(100) 2 X 1 have observed vibrational features between  $3650\text{ cm}^{-1} - 3735\text{ cm}^{-1}$  attributed to the SiO-H vibrational stretching mode. Infrared studies of SiOH species on silica surfaces have observed SiO-H vibrational features between  $3540 - 3750\text{ cm}^{-1}$ . The frequency of SiO-H stretching vibration depends on the degree of hydrogen bonding between the OH groups. The higher the degree of

hydrogen bonding, the lower the absorption frequency.

Infrared features at  $3745 - 3750 \text{ cm}^{-1}$  on silica have been assigned to isolated single SiOH species (41). Infrared features at  $3650 - 3660 \text{ cm}^{-1}$  on silica have been identified as adjacent pairs of SiOH groups that are hydrogen-bonded to each other (41). The infrared feature at  $3680 \text{ cm}^{-1}$  in Fig. 1 approximates the frequency expected from isolated pairs of SiOH species. Similarly, the absorption feature at  $2707 \text{ cm}^{-1}$  in Fig. 2 is consistent with the isotope shift anticipated from the SiO-D stretching vibration.

Electron energy loss features at  $775 \text{ cm}^{-1} - 820 \text{ cm}^{-1}$  after  $\text{H}_2\text{O}$  exposure have been previously assigned to a combination of the Si-OH stretch and the SiO-H bend by several HREELS studies (4,5). Our thermal annealing studies will show that infrared features at this wavelength are also produced by Si-H bending modes where the silicon is backbonded to oxygen atoms. In contrast, the thermal annealing studies after  $\text{D}_2\text{O}$  adsorption show a close correspondence between the SiO-D stretch at  $1513 \text{ cm}^{-1}$  and the infrared absorption feature at  $835 \text{ cm}^{-1}$ . This correlation suggests that the absorption feature at  $835 \text{ cm}^{-1}$  after  $\text{D}_2\text{O}$  adsorption is produced solely by a Si-OD stretching vibration and is not affected by Si-D bending modes.

After a  $\text{H}_2\text{O}$  exposure at 300 K, the infrared spectrum shows clear evidence of silicon hydride and silicon hydroxyl dissociation products. No evidence of molecular  $\text{H}_2\text{O}$ , such as the  $\text{H}_2\text{O}$  bending mode at  $1594 \text{ cm}^{-1}$ , was observed in the infrared spectrum. Despite early evidence for molecular adsorption (1-3), similar dissociation products have been monitored in HREELS studies of  $\text{H}_2\text{O}$  on Si (111)  $7 \times 7$  (4,5) and Si(100)  $2 \times 1$  (5) and multiple total-internal-reflectance infrared studies of  $\text{H}_2\text{O}$  on Si(100)  $2 \times 1$  (11). These recent vibrational studies all argue against molecular adsorption.

The infrared spectrum of porous silicon after  $\text{H}_2\text{O}$  adsorption at 300 K is almost identical to the HREELS spectra obtained after  $\text{H}_2\text{O}$  adsorption on Si(100)  $2 \times 1$  (5) and Si(111)  $7 \times 7$  (4, 5). The close correspondence in vibrational spectral features and frequencies demonstrates that porous silicon surfaces are very similar to single-crystal silicon surfaces. This similarity suggests

that high-surface area porous silicon surfaces can be employed to study silicon surface chemistry.

## B. Adsorption and Thermal Annealing Studies

The thermal annealing studies in Figs. 3-6 show that the SiOH and SiOD surface species have decomposed after annealing above 600 K. The infrared spectra in Figs. 3 and 4 and the integrated absorbance measurements in Figs. 5 and 6 reveal that the decrease in the SiOH species is accompanied by the concurrent growth of SiH and SiOSi species. This growth is clearly observed by the increased absorption in both the Si-H stretching region and in the Si-O-Si asymmetric stretch region between 900- 1100  $\text{cm}^{-1}$ .

The decrease in the SiOH species between 400-600 K is also in good agreement with a recent laser-induced thermal desorption (LITD) study of  $\text{H}_2\text{O}$  decomposition on Si(111) 7x7 (42). In this study, SiOH LITD products were observed after saturation  $\text{H}_2\text{O}$  exposures (42). Temperature-programmed LITD studies revealed that the SiOH LITD signals persisted until temperatures of 600 K. The correlation between these FTIR results and the earlier LITD studies will be discussed in detail elsewhere (43).

Figure 3 reveals that the SiH species increase as the SiOH species decrease. The thermal annealing results in Figs. 5 and 6 show that the maximum integrated absorbance for the Si-H (Si-D) stretching vibration is reached at 650 K. At this temperature, the integrated absorbance of the Si-H (Si-D) stretching vibration is approximately twice the initial Si-H (Si-D) integrated absorbance at 300 K. Assuming complete dissociation, a saturation  $\text{H}_2\text{O}$  exposure would be expected to produce equivalent amounts of surface SiOH and SiH species, i.e.  $\text{H}_2\text{O} \rightarrow \text{SiH} + \text{SiOH}$ . Consequently, the twofold increase in the integrated absorbance of Si-H (Si-D) stretching vibration is consistent with a complete conversion of surface hydroxyl species, i.e.  $\text{SiOH} \rightarrow \text{SiH} + \text{SiOSi}$ , and an overall reaction of  $\text{SiH} + \text{SiOH} \rightarrow 2\text{SiH} + \text{SiOSi}$ .

Above 650K, the absorbance of the Si-H (Si-D) stretching vibration decreases. This decrease is consistent with  $\text{H}_2$  ( $\text{D}_2$ ) desorption from silicon surfaces (27-29). Moreover, at annealing temperatures between 300 K - 640 K, no increase in the background pressure of  $\text{H}_2$  was

observed by the mass spectrometer. This behavior indicates that hydrogen atoms must be transferred to the silicon surface during SiOH decomposition.

The increase in the integrated absorbance of the Si-H stretching vibration as the surface is annealed from 300 K to 640 K is also consistent with the SiH uptake kinetics shown in Fig. 7. The saturation number of SiH species obtained at 600 K is approximately twice the amount obtained at 300 K. This difference is produced by the different thermal stabilities of the SiOH species at these two temperatures. At 600 K, the SiOH species decomposes to yield SiOSi and SiH species. At 300 K, the SiOH species is stable and the hydrogen remains in the SiOH species.

The two-fold increase in the integrated absorbance of the Si-H stretching vibration argues that the surface reaction is  $\text{SiH} + \text{SiOH} \rightarrow 2\text{SiH} + \text{SiOSi}$ . The factor of two increase suggests that the infrared cross section for the Si-H stretching vibration remains constant versus surface hydrogen coverage. This constant cross section is in agreement with previous infrared studies that demonstrated that the disappearance of the integrated absorbance of the Si-H stretching vibration correlated well with the  $\text{H}_2$  desorption yield (27).

Fig. 8 reveals that five times more oxide is formed after  $\text{H}_2\text{O}$  exposure at 800 K compared with a similar  $\text{H}_2\text{O}$  exposure at 600 K. The increased growth of the absorbance of the Si-O-Si stretching vibration at 800 K can be explained by hydrogen site-blocking. The surface oxide coverage is limited by surface hydrogen at 600 K because the hydrogen ties up available surface dangling bonds. At 800 K,  $\text{H}_2$  desorbs and dangling-bond surface sites are available for more  $\text{H}_2\text{O}$  adsorption and additional SiOSi species. Previous  $\text{O}_2$  oxidation studies on Si(111) 7x7 have also observed that both the saturation oxide coverage and initial oxidation rate decrease as a function of preadsorbed hydrogen coverage (44).

### C. Effects of Surface Oxide on the Hydrogen Vibrational Spectra

Previous HREELS studies of  $\text{H}_2\text{O}$  on Si(111) 7x7 (4) have observed an energy loss feature at  $775 \text{ cm}^{-1}$  that is in excellent agreement with the infrared absorption at  $775 \text{ cm}^{-1}$  on porous silicon after  $\text{H}_2\text{O}$  adsorption. The energy loss peak at  $775 \text{ cm}^{-1}$  was attributed to both a Si-OH stretch and

SiO-H bend that absorb at approximately at the same frequency (4). For D<sub>2</sub>O adsorption on porous silicon, infrared absorption features for the Si-OD stretch and the SiO-D bend are observed at 835 cm<sup>-1</sup> and 617 cm<sup>-1</sup>. These two infrared features are in agreement with the energy loss peaks at 835 cm<sup>-1</sup> and 610 cm<sup>-1</sup> monitored in the previous HREELS study of D<sub>2</sub>O decomposition Si(111) 7x7 (4).

The thermal behavior of the 775 cm<sup>-1</sup> infrared absorption peak observed after H<sub>2</sub>O adsorption is shown in Fig. 5. The temperature-dependent changes indicate that this absorption is not dependent solely on the overlapping features from the Si-OH stretch and the SiO-H bend. If the 775 cm<sup>-1</sup> absorption peak is only attributed to a combination of the Si-OH stretch and SiO-H bend, then this feature should correlate well with the SiO-H stretching mode at 3680 cm<sup>-1</sup>. Fig. 5 clearly shows that the absorbance at 775 cm<sup>-1</sup> does not decrease over the same temperature range as the absorbance corresponding to the SiO-H stretching mode at 3680 cm<sup>-1</sup>. The 775 cm<sup>-1</sup> absorption feature persists until H<sub>2</sub> thermally desorbs at 800 K. This persistence suggests that the 775 cm<sup>-1</sup> absorption feature is also associated with a Si-H vibrational or bending mode.

Fig. 10a shows the Si-H stretching region of the infrared spectrum after O<sub>2</sub> exposure on a partially hydrogen-covered porous silicon surface. The oxidation was carried out using an O<sub>2</sub> pressure of 1 X 10<sup>-5</sup> Torr for 7 min. with the porous silicon sample at 600 K. No infrared features were observed between 3600 - 3700 cm<sup>-1</sup>. This absence indicates that there are no hydroxyl species produced by O<sub>2</sub> oxidation of the partially hydrogen-covered porous silicon surface.

Infrared features at 2100 cm<sup>-1</sup> - 2300 cm<sup>-1</sup> in the Si-H stretching region and at 900 cm<sup>-1</sup> - 1100 cm<sup>-1</sup> in the Si-O-Si stretching region are observed as shown in Fig 10. These absorptions indicate that SiH and SiOSi species predominate on the surface. Following O<sub>2</sub> exposure, an additional infrared feature is observed in Fig. 10b at 777 cm<sup>-1</sup>. The thermal stability of this 777 cm<sup>-1</sup> absorption feature was very similar to the thermal stability of the 775 cm<sup>-1</sup> infrared feature produced after H<sub>2</sub>O exposure shown in Fig. 5. These results suggest that the absorption at 777 cm<sup>-1</sup> in Fig. 10b is an oxygen-induced blue-shift of the Si-H wagging mode at 620 cm<sup>-1</sup> (45).

Previous studies on oxidized amorphous silicon have observed absorption features at 780

$\text{cm}^{-1}$ ,  $850 \text{ cm}^{-1}$  and  $875 \text{ cm}^{-1}$  (46). These infrared features were attributed to modes derived from a coupling of Si-H and Si-O-Si motions (46). After the exposure of  $\text{O}_2$  to the hydrogen-covered porous silicon surface, similar infrared features are observed in Fig. 10b at  $777 \text{ cm}^{-1}$ ,  $820 \text{ cm}^{-1}$  and  $857 \text{ cm}^{-1}$ . These blue-shifted Si-H wagging mode absorption features are believed to be correlated with SiH species backbonded to one, two or three oxygen atoms, as discussed below.

Blue-shifted absorption features in the Si-H stretching region between  $2100 - 2250 \text{ cm}^{-1}$  produced by silicon oxidation have been observed in amorphous silicon (47-49). An HREELS study of Si(100)  $2 \times 1$  has also observed a blue-shift in the Si-H stretching frequency from  $2104 \text{ cm}^{-1}$  to  $2282 \text{ cm}^{-1}$  versus oxygen coverage. Moreover, infrared spectra of gas-phase-substituted silane molecules  $\text{SiHR}_1\text{R}_2\text{R}_3$  have shown that the vibrational frequency blue-shifts in a systematic way with the electronegativity of substituting groups (50, 51). For example, the Si-H infrared frequency of  $(\text{CH}_3)_2\text{HSiOSi}(\text{CH}_3)_3$ ,  $(\text{C}_2\text{H}_5\text{O})_2\text{HSiCH}_3$  and  $(\text{CH}_3\text{O})_3\text{SiH}$  are  $2097 \text{ cm}^{-1}$ ,  $2165 \text{ cm}^{-1}$  and  $2203 \text{ cm}^{-1}$ , respectively (51).

Blue-shifts of the frequency of the Si-H stretching vibration have also been observed for other electronegative substituents (50). In addition, microwave spectroscopy experiments on gas-phase-substituted silane molecules have observed a decrease in the Si-H bond length as a function of increasing number of substituent fluorine atoms (50, 52, 53). These previous investigations indicate that electronegative elements withdraw electron density from the silicon atom and subsequently decrease the Si-H bond length and increase the Si-H vibrational frequency.

In view of these earlier studies, the absorption features at  $2176 \text{ cm}^{-1}$  and  $2268 \text{ cm}^{-1}$  in Fig. 10a are assigned to SiH species backbonded to two and three oxygen atoms, respectively. Likewise, the absorption peaks at  $2176 \text{ cm}^{-1}$  and  $2268 \text{ cm}^{-1}$  in Fig. 9b after  $\text{H}_2\text{O}$  exposure and annealing to  $640 \text{ K}$  are assigned to SiH surface species backbonded to two or three oxygen atoms, respectively. The shoulder at  $2119 \text{ cm}^{-1}$  on the main Si-H absorption feature at  $2102 \text{ cm}^{-1}$  in Fig. 9b is assigned to a Si-H surface species backbonded to one oxygen atom.

The proposed SiH surface species backbonded to one, two or three oxygen atoms are

consistent with previous XPS and AES observations (27,54-57). These XPS and AES measurements have revealed a distribution of silicon oxidation states on oxygen-covered silicon surfaces at submonolayer oxygen coverages (27,54-57). Si(I), Si(II), Si(III) and Si(IV) species have all been monitored where the numeral designates the number of oxygen atoms bound to the silicon atom (54-56). The distribution of silicon oxidation states favors the lower oxidation numbers at low oxygen coverages and progressively shifts to higher oxidation numbers at higher oxygen coverage.

## V. Conclusions

The decomposition of H<sub>2</sub>O and D<sub>2</sub>O on porous silicon surfaces was studied using transmission Fourier-transform infrared (FTIR) spectroscopy. The FTIR spectra revealed that H<sub>2</sub>O (D<sub>2</sub>O) dissociates upon adsorption at 300 K to form SiH (SiD) and SiOH (SiOD) groups, i.e., H<sub>2</sub>O → SiOH + SiH. The decomposition of the surface species formed from H<sub>2</sub>O (D<sub>2</sub>O) adsorption was then monitored using the Si-H (Si-D) stretch at 2100 cm<sup>-1</sup> (1518 cm<sup>-1</sup>), the SiO-H (SiO-D) stretch at 3680 cm<sup>-1</sup> (2713 cm<sup>-1</sup>) and the Si-O-Si stretch at 900 cm<sup>-1</sup> - 1100 cm<sup>-1</sup>.

As the silicon surface was progressively annealed to 650 K, the FTIR spectra revealed that the SiOH species decomposed to silicon oxide species and additional SiH species. At 650 K, the maximum integrated absorbance for the Si-H (Si-D) stretching vibration was obtained and was approximately twice the integrated absorbance at 300 K. The changes in the integrated infrared absorbances versus temperature were consistent with the reaction SiOH → SiH + SiOSi. Above 650 K, the surface SiH species decreased concurrently with H<sub>2</sub> desorption from the porous silicon surface.

After annealing above 600 K, new blue-shifted infrared features were observed in the Si-H stretching vibration region at 2119 cm<sup>-1</sup>, 2176 cm<sup>-1</sup> and 2268 cm<sup>-1</sup>. Infrared studies of partially hydrogen-covered porous silicon surfaces exposed to O<sub>2</sub> suggested that these blue-shifted Si-H stretching vibrations were associated with silicon atoms backbonded to one, two or three oxygen

atoms, respectively. Similar blue-shifted absorption features in the Si-H wagging region were produced by oxygen adsorption and also attributed to SiH species on silicon atoms backbonded to oxygen atoms.

## **Acknowledgments**

This work was supported by the U.S Office of Naval Research under Contract No. N00014-86-K-545. Some of the equipment utilized in this work was provided by the NSF-MRL through the Center for Material Research at Stanford University. SMG acknowledges the National Science Foundation for a Presidential Young Investigator Award and the A.P. Sloan Foundation for a Sloan Research Fellowship.

## References

1. K. Fujiwara, Surf.Sci.108 (1981) 124.
2. K. Fujiwara and H. Ogata, J. Appl. Phys 48 (1988) 4360.
3. K. Fujiwara, H. Ogata and M. Nishijima, Solid State Commun. 21(1977) 895.
4. M. Nishijima, K. Edamoto, Y. Kubota, S. Tanaka and M. Onchi, J. Chem. Phys. 84 (1986) 6458.
5. H. Ibach, H. Wagner and D. Bruchmann, Solid State Commun.42 (1982) 457.
6. E.M. Oellig, R. Butz, H. Wagner, and H. Ibach, Solid State Commun. 51, (1984) 7.
7. F. Meyer, Surf. Sci. 27 (1971) 107.
8. J.A. Schaefer, J. Anderson, and G.J. Lapeyre, J. Vac. Sci. Technol. A 3 (1985) 1443.
9. J.A. Schaefer, F. Stucki, D.J. Frankel, W. Gopel and G.J. Lapeyre, J. Vac. Sci. Technol. B 2 (1984) 359.
10. F. Stucki, J. Anderson, G.J. Lapeyre and H.H. Farrell, Surf. Sci. 143 (1984) 84.
11. Y.J. Chabal, Phys. Rev. B 29 (1984) 3677.
12. P.A. Schumann Jr., W.A. Keenan, A.H. Tong, H. H. Gegenwarth and C.L. Schneider J. Electrochem Soc. 118 (1971) 145.
13. R.J. Collins and H.Y. Fan Phys. Rev. 93 (1954) 674.
14. L.A. Pugh and K.N. Rao, *Molecular Spectroscopy: Modern Research*, edited by K.N. Rao Academic, New York, 1976), Vol. II.
15. A. Uhlir, Bell Syst. Tech. J 35 (1956) 333.
16. D.R. Turner, J. Electrochem. Soc. 105 (1958) 402.
17. S.F. Chuang, S.D. Collins and R.L. Smith Appl. Phys. Lett 55 (1989) 675.
18. G. Bomchil, R. Herino, K.Barla, and J.C. Pfister, J. Electrochem. Soc. 130 (1983) 1161.
19. K. Barla, R. Herino, G. Bomchil, and J.C. Pfister, J. Cryst. Growth 68 (1984) 727.
20. V. Labunov, V. Bondarenko, L. Glinenko, A. Dorofeev and L. Jabulina, Thin Solid Films 137 (1986) 123.

21. M.I.J. Beale, J.D. Benjamin, M.J. Uren, N.G. Chew and A.G. Cullis, *J. Cryst. Growth* **75** (1986) 408.
22. K. Barla, R. Herino, G. Bomchil J.C. Pfister and A. Freund, *J. Cryst. Growth* **68** (1984) 727 .
23. I.M. Young, M.I.J. Beale and J.E. Benjamin, *Appl. Phys. Lett* **46** (1985) 1133 .
24. R.W. Hardeman, M.I.J. Beale, D.B. Gasson, J.M. Keen, C.Pickering and D.J. Robbins, *Surf. Sci.* **152** , (1985) 1051.
25. K. Barla, G. Bomchil, R. Herino and J.C. Pfister, *J. Cryst Growth* **68**, (1984) 721 .
26. S.Konaka, M. Tabe and T. Sakai, *Appl. Phys. Lett.* **41** (1982) 86.
27. P. Gupta, V.L. Colvin and S.M. George, *Phys. Rev.* **37** (1988) 8234.
28. G. Schulze and M.Henzler, *Surf. Sci.* **124** 336 (1983).
29. B.G. Koehler, C.H. Mak, P.A. Coon, D.A. Arthur and S.M. George, *J. Chem Phys.* **89** (1988) 1709.
30. S.M. George, *J. Vac. Sci. Technol.* **A4** (1986) 2394.
31. G.E. Jellison, *Semiconductors and Semimetals*, Vol. 23: Pulsed Laser Processing of Semiconductors; edited by R.F. Wood, C.W. White, and R.T. Young (Academic Press, New York), Chapter 3.
32. G.G. Macfarlane, T.P. McLean, J.E. Quarrington and V. Roberts, *Phys Rev* **111** (1958) 1245.
33. H.A. Weakliem and D. Redfield, *J. Appl. Phys.* **50** (1979) 1491.
34. P. Gupta, A. S. Bracker, V. L. Colvin and S.M. George, in preparation.
35. E. Fogarassy, A. Slaoui, C. Fuchs and J.L. Regoloni, *Appl. Phys. Lett.* **51** (1987) 337.
36. K. Edamoto, Y. Kubota, H. Kobayashi, M. Onchi and M. Nishijima, *J. Chem Phys.* **83** (1985) 428.
37. Y.J. Chabal and K. Raghavachari, *Phys Rev Lett* **54** (1985) 1055.
38. Y.J. Chabal in *Semiconductor Interfaces: Formation and Properties* (Springer Verlag, NY, 1987).
39. F. Stucki, J.A. Schaefer, J.R. Anderson, G.J. Lapeyre and W. Gopel, *Solid State Comm.* **47**

- (1983) 95.
40. J.A. Schaefer, J. Anderson and G.J. Lapeyre, *J. Vac. Sci. Technol.* **A3** (1985) 1443.
  41. R.K. Iler, *The Chemistry of Silica*, (John Wiley & Sons, New York, 1979), Chap. 6.
  42. B.G. Koehler, C.H. Mak and S.M. George, *Surf. Sci* **221** (1989) 565.
  43. P.Gupta, A.C. Dillon, P.A. Coon and S.M. George *Submitted to Chem. Phys. Lett.*
  44. P. Gupta, C.H. Mak, P.A. Coon and S.M. George, *Phys Rev. B* **40** (1989) 7739.
  45. A.C. Dillon, P. Gupta, M.B. Robinson and S.M. George, *Unpublished.*
  46. G. Lucovsky *Sol. Ener. Mat.* **8** (1982) 165.
  47. P.John, I.M. Odeh, M.J.K. Thomas, M.J. Triccker and J.I.B. Wilson, *Phys. Stat. Sol* **105** (1981) 499.
  48. G. Lucovsky, J. Yang, S.S. Chao, J.E. Tyler and W. Czubytyj, *Phys. Rev B.* **28** (1983) 3225 .
  49. G. Lucovsky, *Solid State Comm.* **29** (1979) 571.
  50. A.L. Smith and N.C. Angelotti, *Spectrochemica Acta*, **15** (1959) 412.
  51. H.W. Thompson, *Spectrochemica Acta*, **16** (1960) 238.
  52. J.D Swalen, B.P Stoicheff, *J. Chem Phys.* **28** (1958) 671.
  53. G.A. Heath, L.F. Thomas and J. Sheridan, *Trans. Faraday Soc.* **50** (1954) 779.
  54. G. Hollinger and F. J. Himpsel, *Phys Rev B* **28** (1983) 3651.
  55. G. Hollinger and F.J. Himpsel, *Appl. Phys Lett.* **44** (1984) 93.
  56. M. Tabe, T.T. Chaing, I. Lindau and W.E. Spicer, *Phys Rev B* **34** (1986) 2706.
  57. K. Edamoto, Y. Kubota, H. Kobayashi, M. Onchi and M. Nishijima, *J. Chem. Phys* **83** (1985) 428.

## Figure Captions

1. Infrared spectrum after a saturation  $\text{H}_2\text{O}$  exposure on porous silicon surfaces at 300 K.
2. Infrared spectrum after a saturation  $\text{D}_2\text{O}$  exposure on porous silicon surfaces at 300 K.
3. Infrared absorbance of a) the SiO-H stretching vibration and b) the Si-H stretching vibration as a function of annealing temperature after a saturation  $\text{H}_2\text{O}$  exposure at 300 K.
4. Infrared absorbance of the Si-OD bending vibration at  $835\text{ cm}^{-1}$  and the Si-O-Si stretching vibration at  $900\text{-}1100\text{ cm}^{-1}$  as a function of annealing temperature after a saturation  $\text{D}_2\text{O}$  exposure at 300 K.
5. Integrated infrared absorbances of the Si-H, Si-OH, SiO-H and Si-O-Si stretching vibrations at  $2090$ ,  $775$ ,  $3680$  and  $980\text{ cm}^{-1}$ , respectively, as a function of annealing temperature after a saturation  $\text{H}_2\text{O}$  exposure at 300 K.
6. Integrated infrared absorbances of the Si-D, SiO-D, Si-OD and the Si-O-Si stretching vibrations at  $1513\text{ cm}^{-1}$ ,  $2707\text{ cm}^{-1}$ ,  $835$  and  $980\text{ cm}^{-1}$ , respectively, as a function of annealing temperature after a saturation  $\text{D}_2\text{O}$  exposure at 300 K.
7. Integrated infrared absorbance of the Si-H stretching vibration at  $2090\text{ cm}^{-1}$  as a function of  $\text{H}_2\text{O}$  exposure on porous silicon surfaces at temperatures of 300 K and 600 K.
8. Integrated infrared absorbance of the Si-O-Si stretching vibration at  $900\text{ - }1100\text{ cm}^{-1}$  as a function of  $\text{H}_2\text{O}$  exposure on porous silicon surfaces at temperatures of 600 K and 800 K.
9. Infrared spectrum in the Si-H stretching region after a) a saturation  $\text{H}_2\text{O}$  exposure at 300 K and b) subsequent annealing to 640 K. New blue-shifted features are

observed at  $2119\text{ cm}^{-1}$ ,  $2176\text{ cm}^{-1}$  and  $2268\text{ cm}^{-1}$ .

10. Infrared spectrum after  $\text{O}_2$  exposure to a partially hydrogen-covered porous silicon surface at 600 K. a) Si-H stretching region where new blue-shifted features are observed at  $2176\text{ cm}^{-1}$  and  $2268\text{ cm}^{-1}$ . b) Si-H bending region where new blue-shifted features are observed at  $777$ ,  $820$ ,  $857\text{ cm}^{-1}$ .

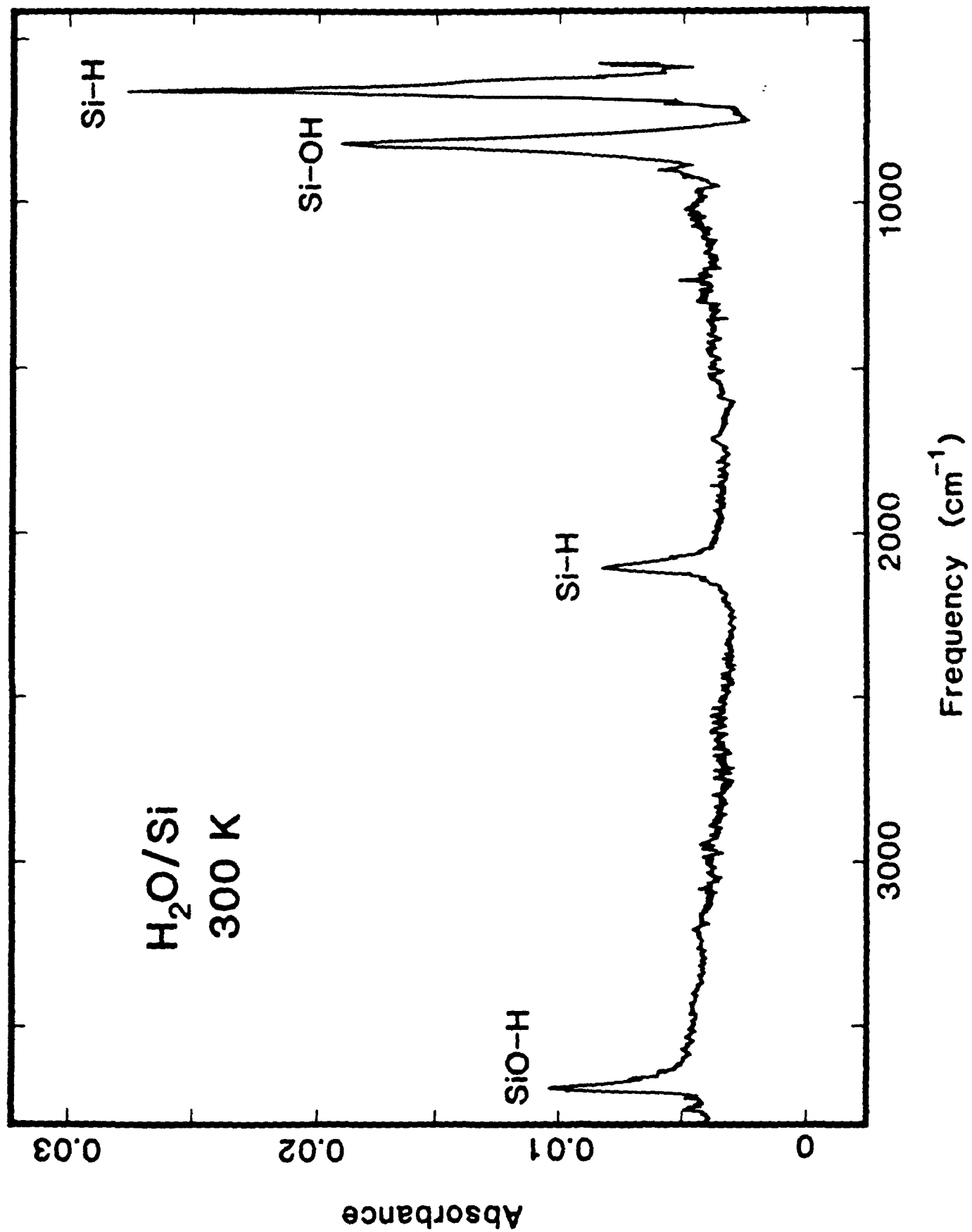


Figure 1

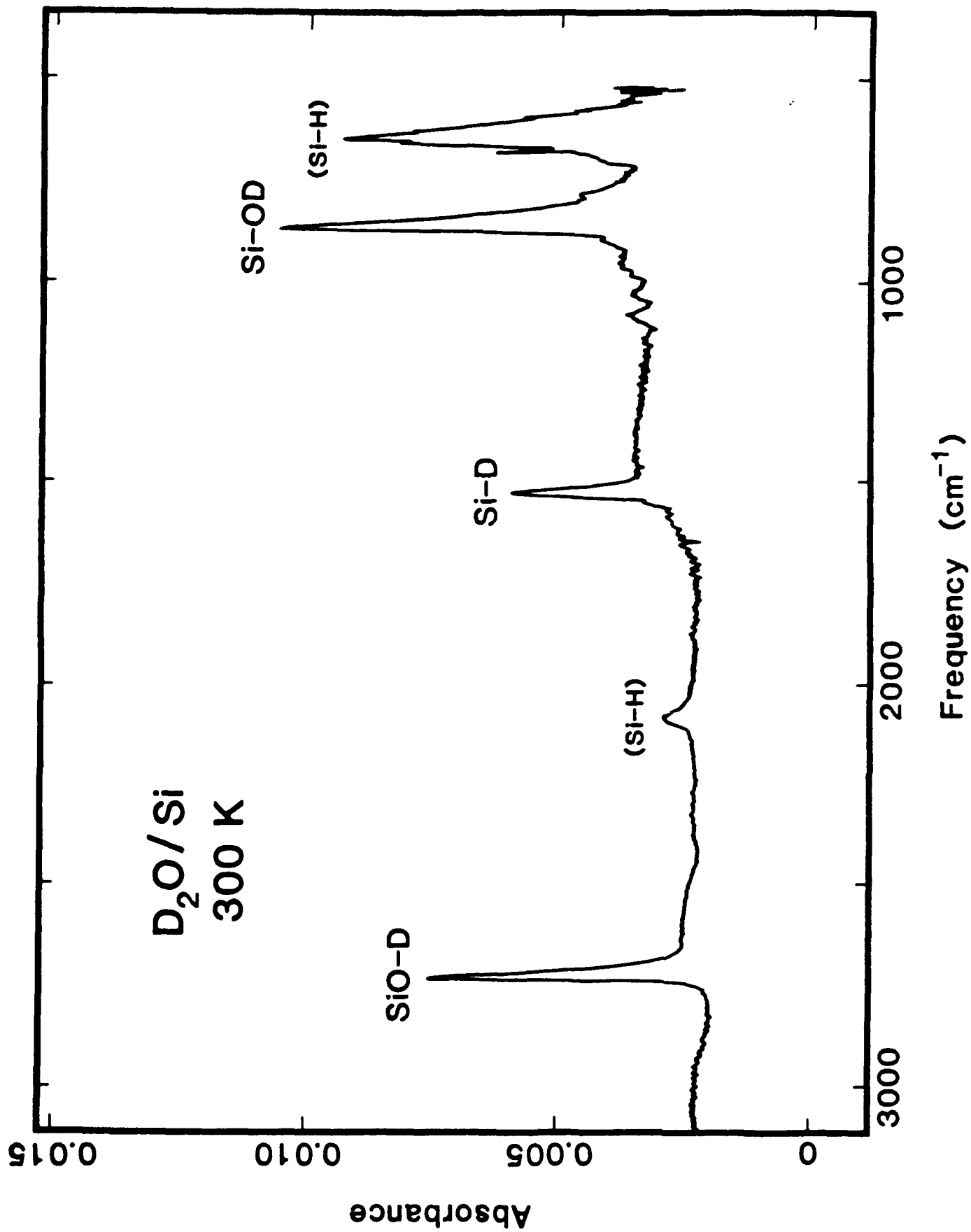


Figure 2

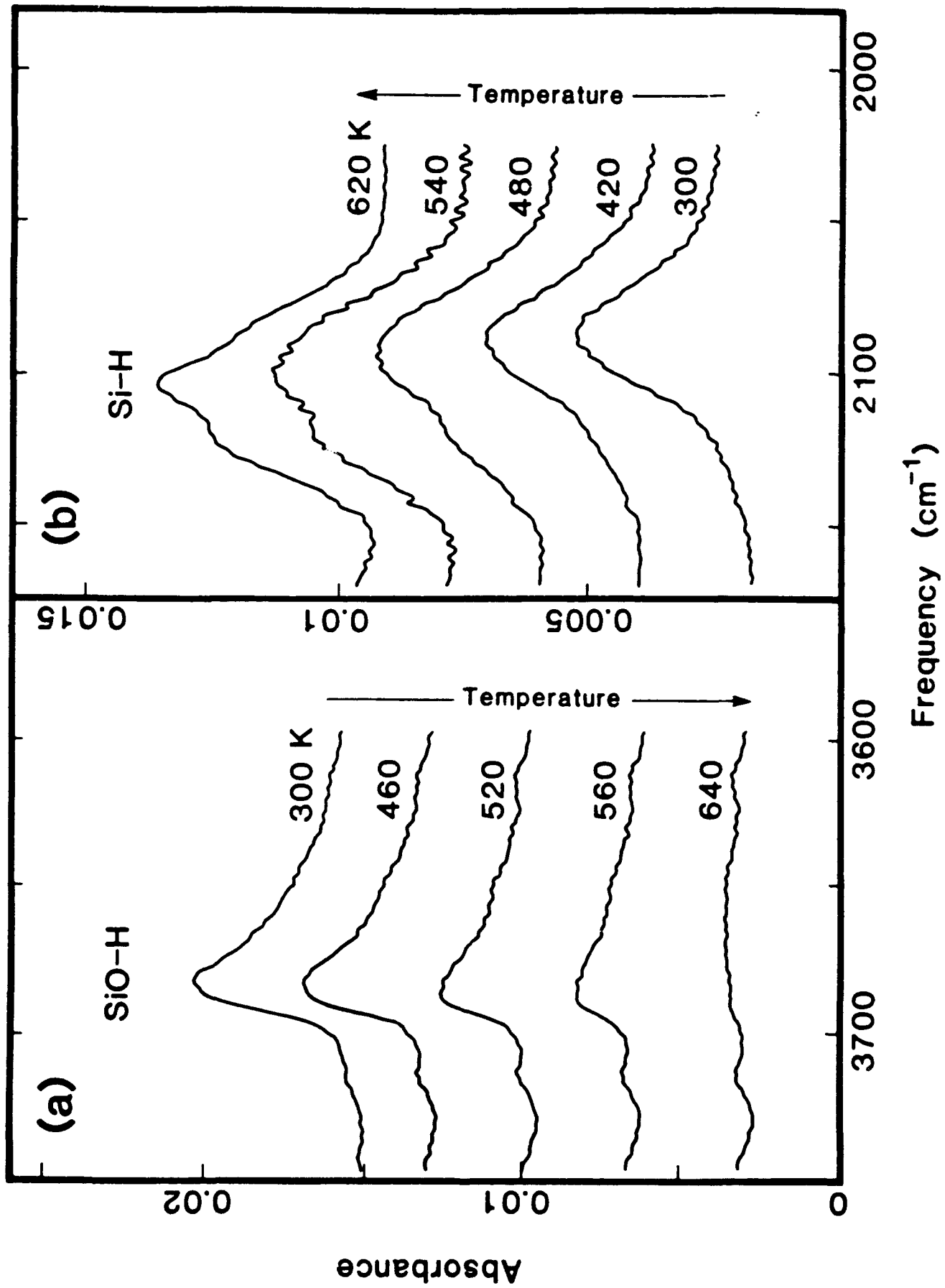


Figure 3

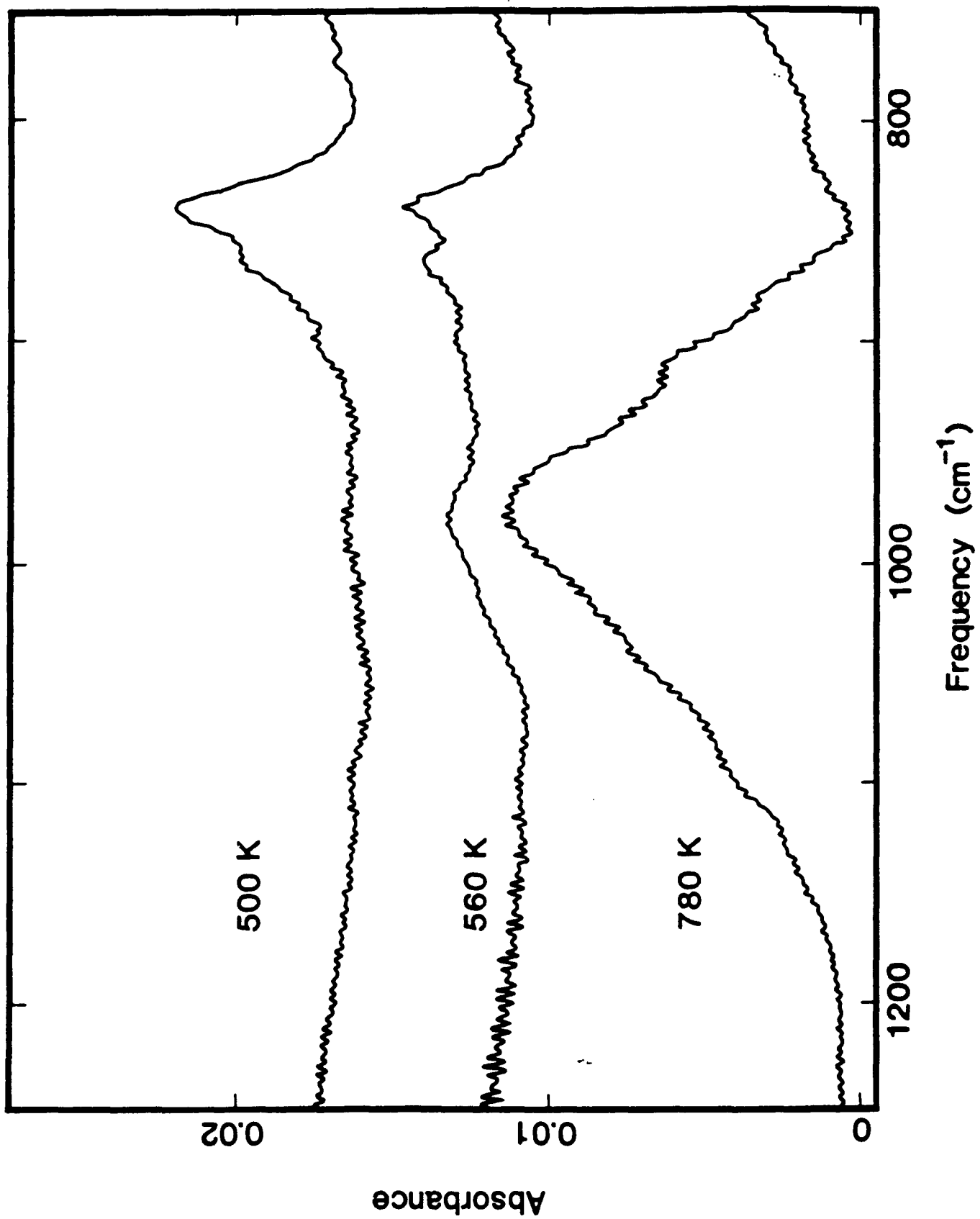


Figure 4

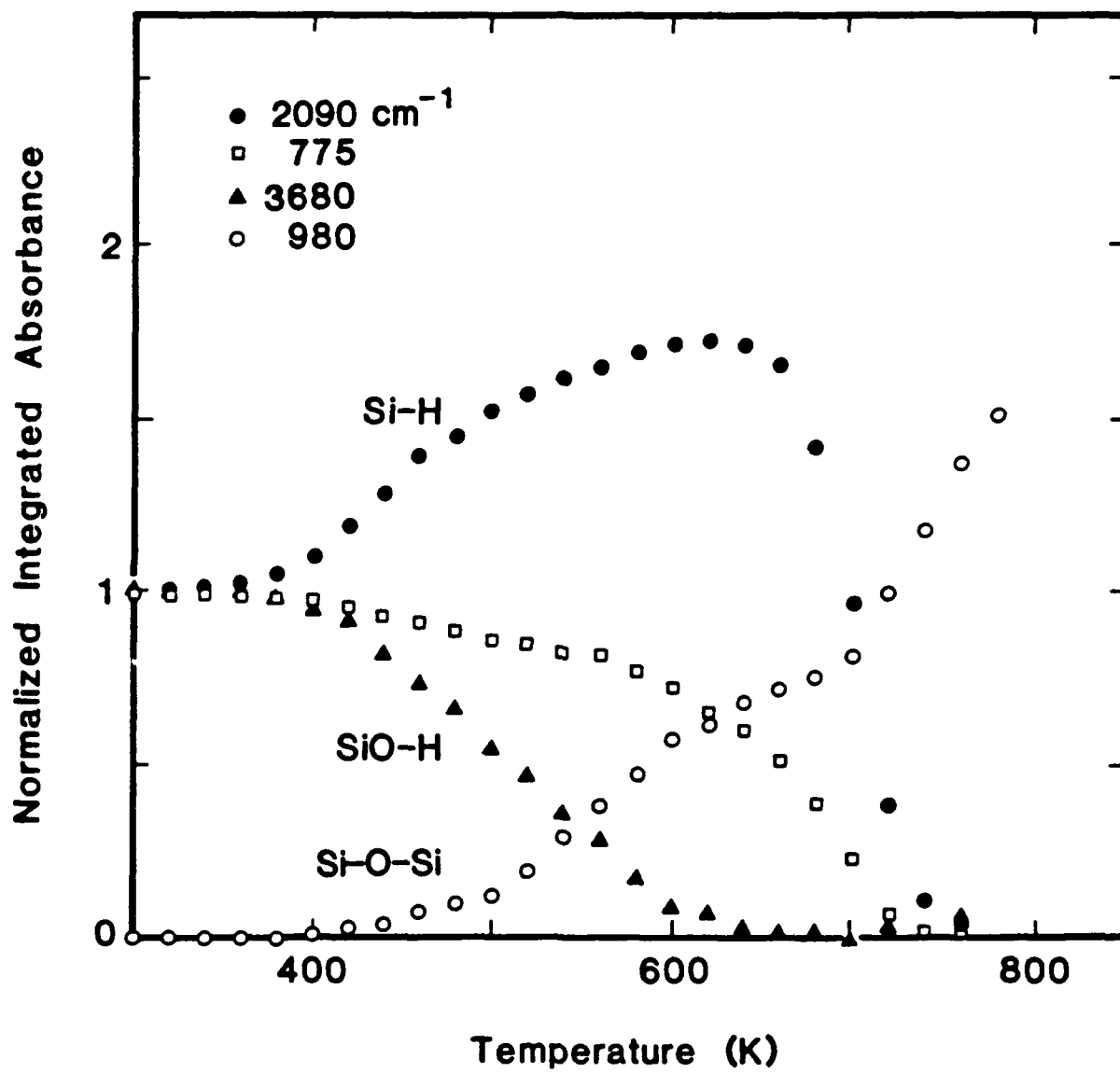


Figure 5

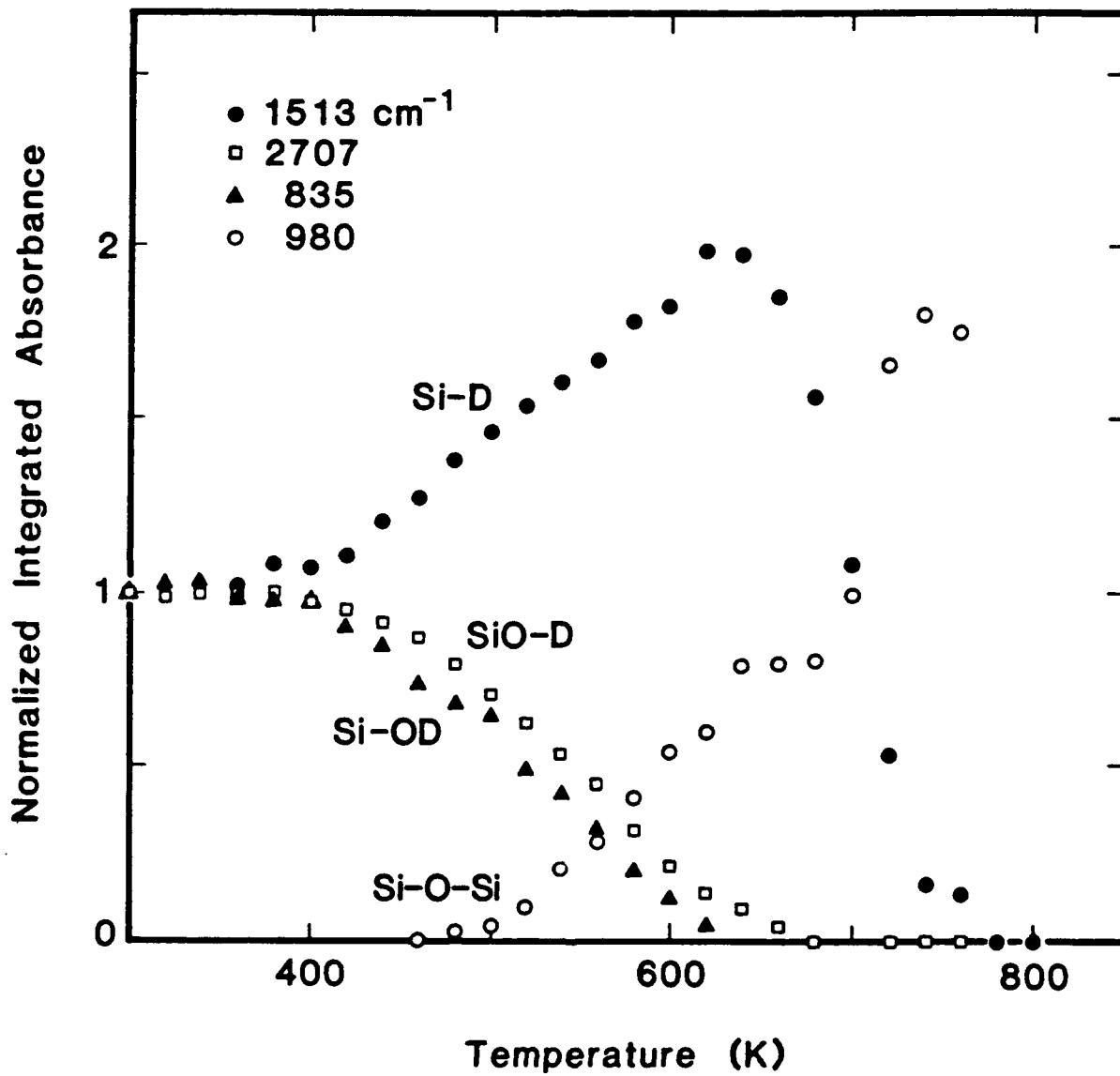


Figure 6

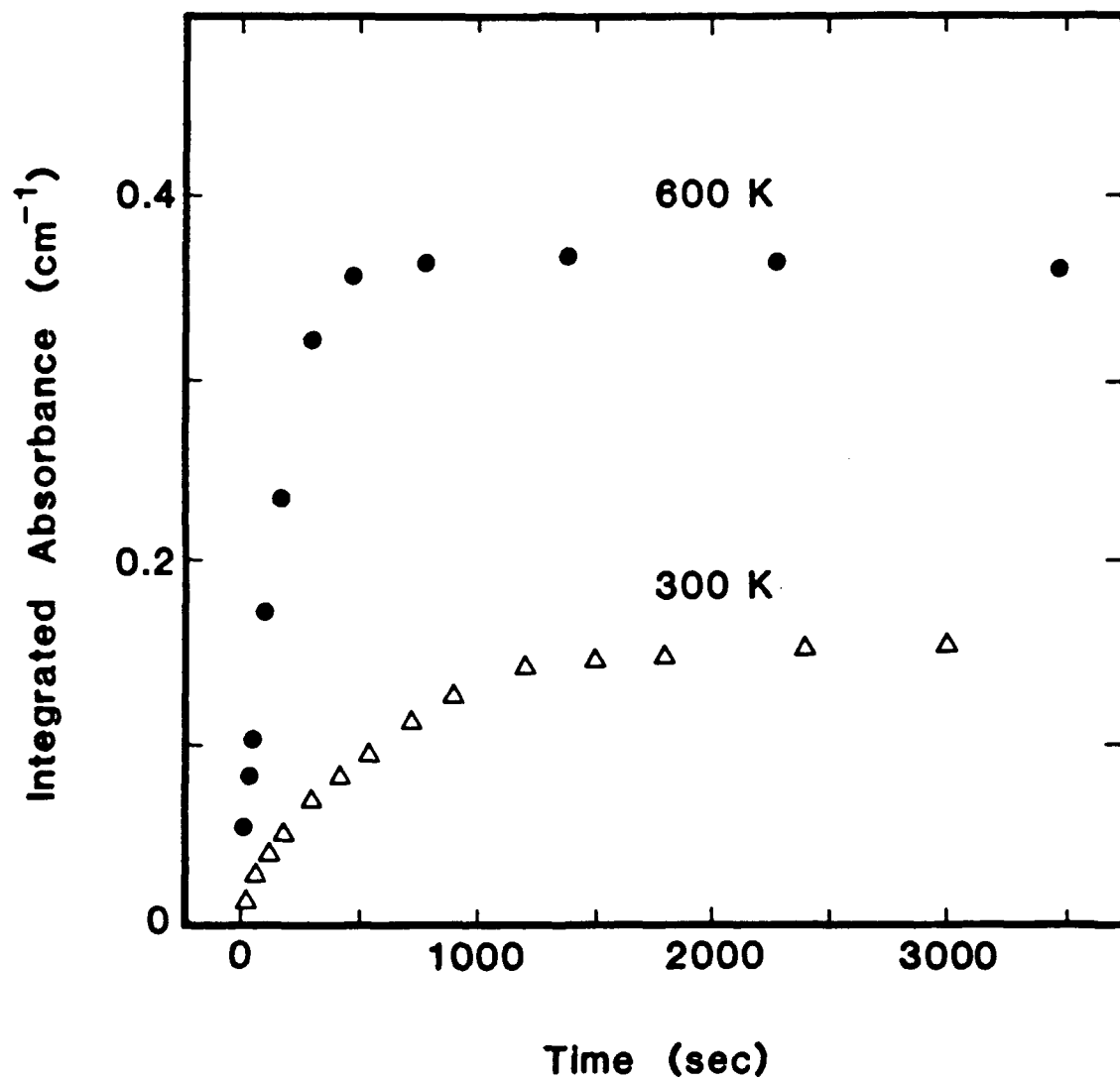


Figure 7

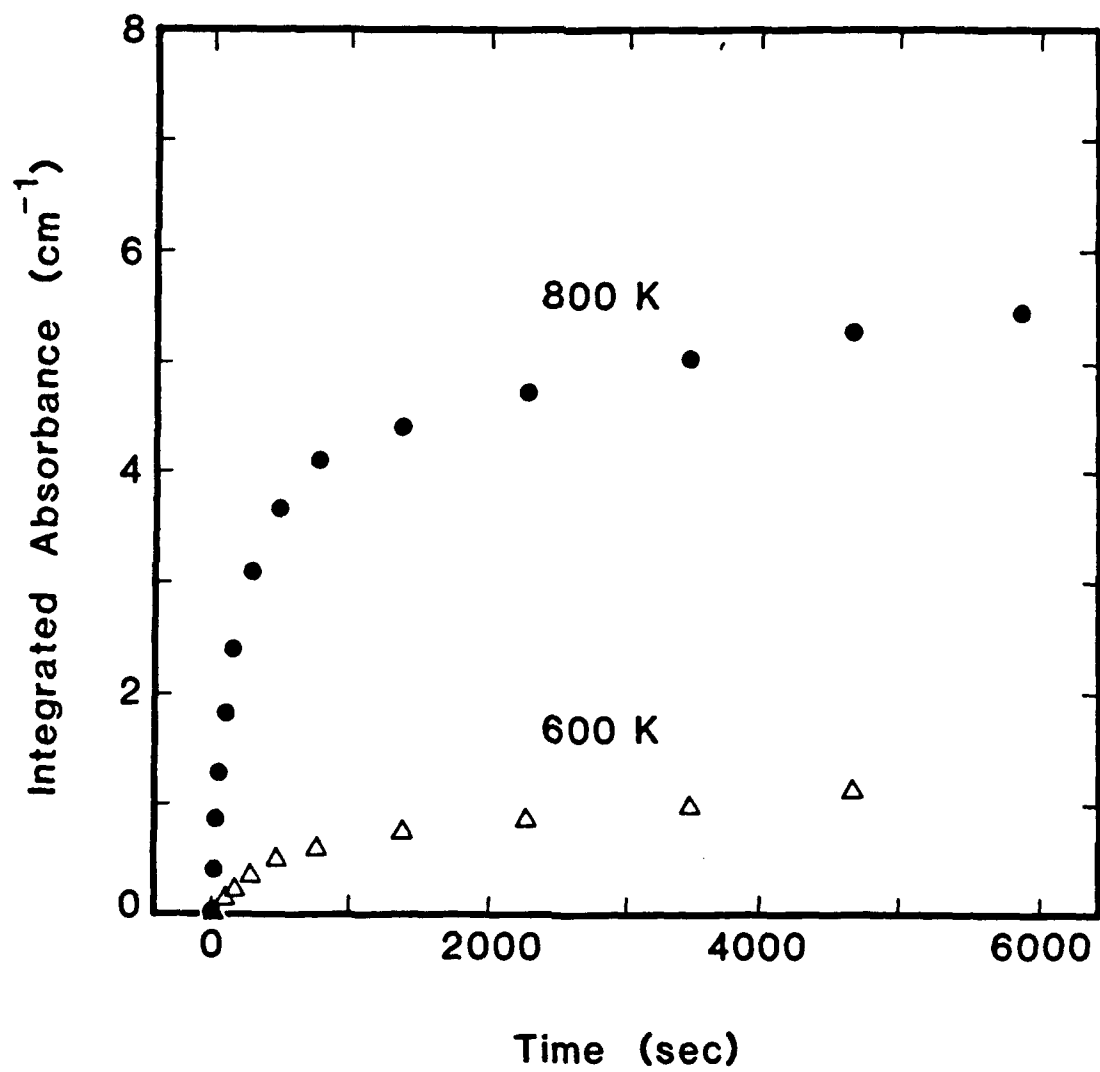


Figure 8

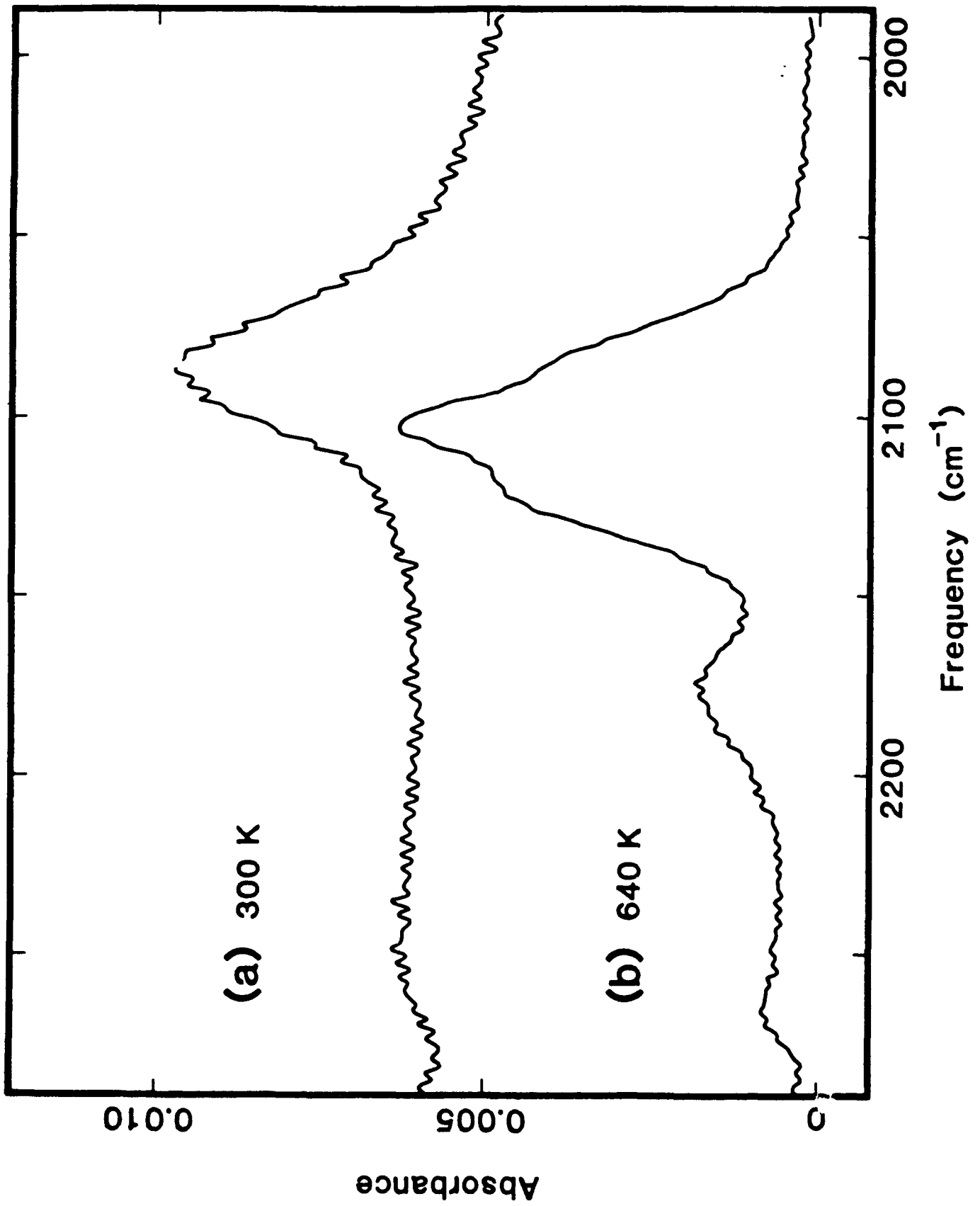


Figure 9

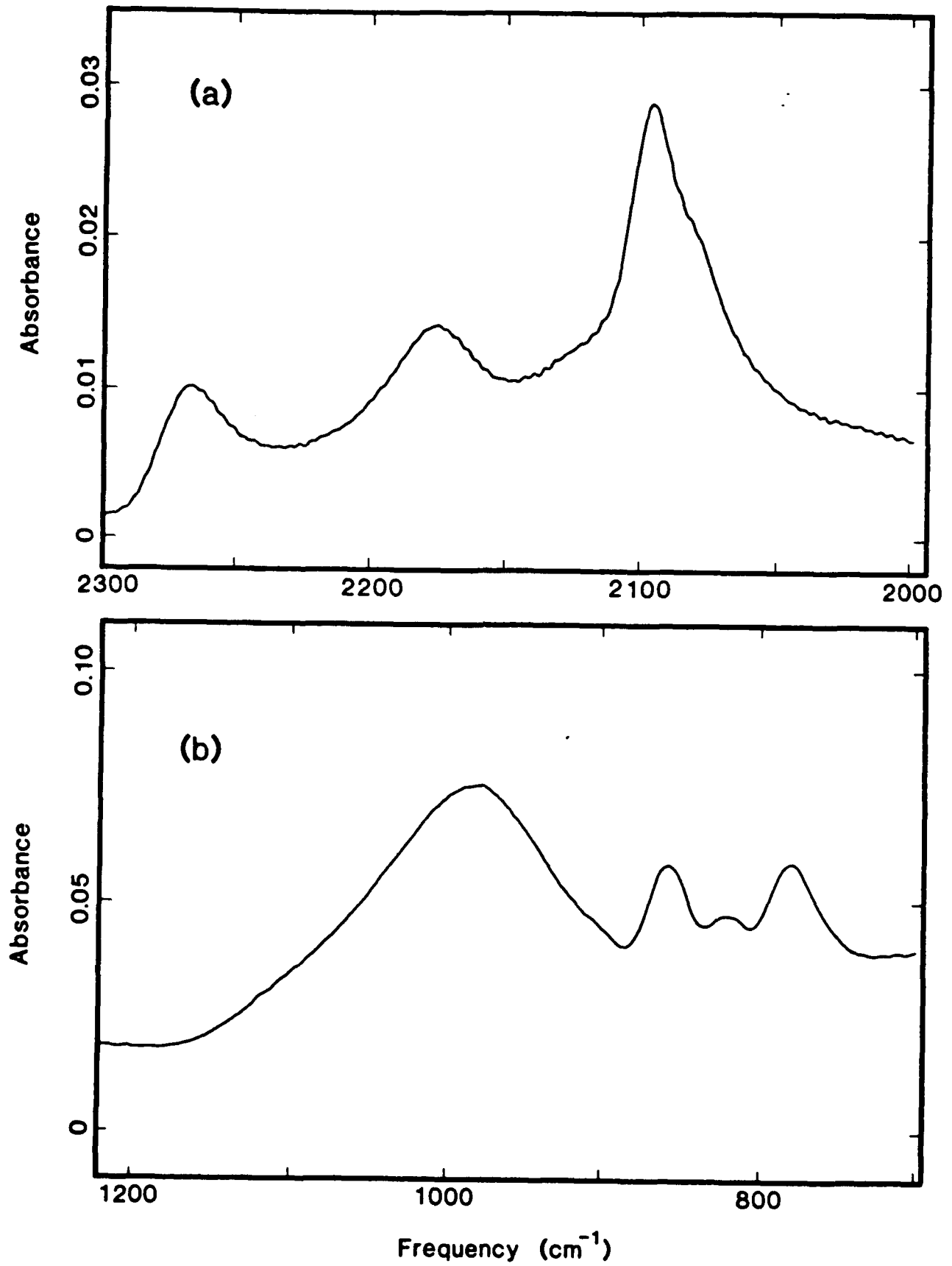


Figure 10